ACS APPLIED MATERIALS & INTERFACES

Research Article

Cite This: ACS Appl. Mater. Interfaces 2018, 10, 15477−15486

www.acsami.org

Design of Nanofiber Coatings for Mitigation of Microbial Adhesion: Modeling and Application to Medical Catheters

Zhou Ye,[†,⊥] AhRam Kim,[†,⊥] Carolyn Y. Mottley,[‡] Michael W. Ellis,[†,§] Candace Wall,[∥] Alan R. Esker,[§,∥] Amrinder S. Nain,[†,‡,§] and Bahareh Behkam*[,†,‡,§]

[†]Department of Mechanical Engineering, [‡]School of Biomedical Engineering & Sciences, [§]Macromolecules Innovation Institute, and [∥]Department of Chemistry, Virginia Tech, Blacksburg, Virginia 24061, United States

Supporting Information

ABSTRACT: Surface-associated microbial communities, known as biofilms, pose significant challenges in clinical and industrial settings. Micro-/nanoscale substratum surface features have been shown to disrupt firm adhesion of planktonic microbes to surfaces, thereby interfering with the earliest stage of biofilm formation. However, the role of geometry and size of surface features in microbial retention is not completely understood. In this study, we developed a biophysical model that describes the changes in the total free energy (adhesion energy and stretching energy) of an adherent *Candida albicans* cell on nanofiber-coated surfaces as a function of the geometry (i.e., diameter) and configuration (i.e., interfiber spacing) of the surface features (i.e., nanofibers). We then introduced a new nondimensional parameter, Π, to represent the ratio of cell rigidity to cell−substratum interfacial energy. We show that the total free energy is a strong function of topographical feature size at higher Π and lower spacing values. To confirm our biophysical model predictions, we performed 24 h dynamic retention assays and quantified cell attachment number density on surfaces coated with highly ordered polystyrene nanofibers. We show that the total free energy of a single adherent cell on a patterned surface is a key determinant of microbial retention on that surface. The cell attachment density trend closely correlates with the predictions based on the adherent single-cell total energy. The nanofiber coating design (1.2 μm diameter, 2 μm spacing) that maximized the total energy of the adherent cell resulted in the lowest microbial retention. We further demonstrate the utility of our biophysical model by showing close correlation between the computed single-cell total free energy and biofilm nucleation on fiber-coated urinary and central venous catheters of different materials. This biophysical model could offer a powerful new paradigm in ab initio design of patterned surfaces for controlled biofilm growth for medical applications and beyond.

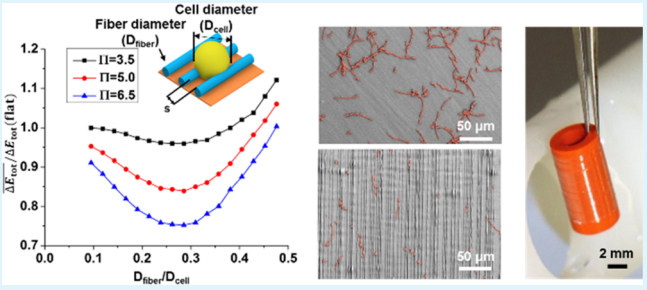

KEYWORDS: *microbial adhesion, microbial retention, adhesion model, stretching energy, biofilm, surface topography, patterned surfaces*

1. INTRODUCTION

Biofilm is a multicellular community of microbes embedded in a matrix of extracellular polymeric substance with increased resistance to antimicrobials and immune system.[1,2] Biofilm formation on surfaces adversely affects function in a variety of applications, including food processing,[3] wastewater treatment,[4] industrial vessels and pipes,[5,6] and medical implants and devices.[7,8] In particular, biofilm formation on medical devices is responsible for a substantial portion of the healthcare-associated infections, which cause approximately 100 000 deaths and an estimated $28−$45 billion in added healthcare costs per annum.[9]

Given the long-standing challenges of biofilm eradication, biocidal, and antiadhesion coatings that inhibit biofilm formation a priori are continuously being explored.[10] These surface modification strategies aim to disrupt the ability of planktonic microbes to firmly adhere to surfaces, thereby interfering with the earliest stage of biofilm formation. One such strategy is based on modification of surface topography to make surfaces unfavorable for microbial adhesion. It has been widely demonstrated that micro-/nanoscale surface topography influences microbial attachment,[11−15] biofilm formation[16,17] (for comprehensive reviews of the role of surface topography and other characteristics in microbial retention and biofilm formation, refer to refs 18−22), and even viability.[23,24] The role of surface structure geometry, dimensions, and configuration on microbial retention is only partially understood, and a quantitative framework that enables ab initio design of surface patterns that optimally inhibits microbial adhesion is currently lacking. Development of such a theoretical framework can offer a powerful new paradigm in antifouling biomaterial design and

Received: February 17, 2018
Accepted: April 11, 2018
Published: April 11, 2018

DOI: 10.1021/acsami.8b02907
ACS Appl. Mater. Interfaces 2018, 10, 15477−15486

significantly enhance the current tedious and iterative design process by refining the experimental design space.

In the past, several approaches have been used to model early-stage reversible microbial adhesion. Perhaps the most well known is the Derjaguin−Landau−Verwey−Overbeek (DLVO) theory of colloid stability, which has been extended to microbial adhesion. The DLVO theory describes the cell−substratum interactions as a balance of long-range Lifshitz−van der Waals interactions and electrostatic double-layer interactions.[25] The DLVO theory can qualitatively explain the influence of the ionic strength of the culture medium[26,27] and the substratum charge density[28,29] but cannot explain the experimentally measured forces in high ionic strength or high pH media wherein the hydration force is significant.[30,31] The extended DLVO (XDLVO) theory was established to include the short-range Lewis acid−base interaction from hydrogen bonding at the microbial−substratum interface. Compared to the DLVO theory, the XDLVO theory has been shown to more accurately predict microbial adhesion behaviors.[32−34] Surface thermodynamic-based approaches have also been developed to model microbial adhesion by describing the cell−substratum interactions in terms of the adhesion free energy (ΔG_{ad}).[35−37] Adhesion is considered to be energetically favorable for $\Delta G_{ad} < 0$ and unfavorable for $\Delta G_{ad} > 0$, although it has been shown that the adhesion may occur even under energetically unfavorable conditions.[38] All of the aforementioned models treat microorganisms as rigid particles without considering the stretching and deformation of the cell and the associated energy change. The cell wall stretching can be significant for microorganisms with relatively low stiffness (e.g., yeast) or in the presence of closely spaced and high aspect ratio micro-/nanoscale surface patterns. For instance, significant deformation and stretching of the cell wall are believed to be responsible for the antimicrobial activity of nanopatterns on the cicada wing surface.[23,24] Thus, the energy changes due to both adhesion and cell wall stretching must be included in modeling microbial adhesion on micro-/nanopatterned surfaces, nonetheless, the role of the stretching energy on cell adhesion has been rarely explored.

It should be noted that none of the classical theories are capable of describing the adhesion outcome for all conditions, and the development of a comprehensive adhesion model remains a matter of active research.[38,39] Our goal here is more focused, however. We hypothesize that the total free energy of a single adherent cell is a key determinant of the microbial retention density outcome on patterned surfaces. If proven, the patterned surface on which the adherent cell's total energy is the highest (i.e., least favorable for cell attachment), will have the lowest cell attachment density. To test this hypothesis, we developed a biophysical model that describes changes in the total energy (adhesion and stretching energy) of an adherent cell as a function of the material, geometry, size, and spatial configuration of the surface structures, as well as the cell size and the biophysical properties of the cell wall. We used this model to calculate the change in the total energy of *Candida albicans* yeast (model fungal pathogen, morphology: round, diameter: 4.2 μm) adherent to nanofiber-coated surfaces with uniform fiber diameter and spacing. We theoretically investigate the effect of nanofiber diameter, spacing, and material on the change in the total energy of *C. albicans* adherent cells.

We then fabricated polystyrene (PS) nanofiber-coated PS substrata and conducted experiments to quantify the cell attachment density for varying fiber diameters at prescribed spacing. We show that the trend for attachment density of *C. albicans* on nanofiber-coated substrata of varying diameters closely correlates with our theoretical quantification of the adherent single-cell total free energy. Furthermore, we demonstrate the utility of this experimentally validated model in ab initio biomaterial design by showing the correlation between the single-cell total free energy calculated from the biophysical model and the biofilm nucleation outcome on fiber-coated urinary and central venous catheters of different materials.

2. EXPERIMENTAL SECTION

2.1. Biophysical Model of Cell Adhesion on Patterned Surfaces. *C. albicans* grows either as unicellular yeast or in filamentous pseudohyphal and hyphal forms (Figure S1). *C. albicans* biofilm formation begins with adherence of its yeast form to surfaces, which form a basal layer, followed by growth and proliferation of yeast, pseudohyphal, and hyphal cells.[40−42] As a result, our *C. albicans* early-stage adherence model was developed and demonstrated for the yeast morphology of *C. albicans*. We hypothesize that the total energy of the yeast cell at the early-stage of adherence, which can be highly regulated by the substratum surface topography, dictates the microbial attachment density outcome. To test this hypothesis, we first developed a biophysical model of the adhesion of *C. albicans* yeasts to nanofiber-coated surfaces. The total change in energy (ΔE_{tot}) of an adherent cell relative to its planktonic state is comprised the changes in the adhesion energy (ΔE_{ad}, energy change due to the adhesion of the cell to the substratum), the stretching energy (ΔE_{str}, energy change due to the stretching of the cell wall), and the bending energy (ΔE_c, energy change due to changes in the cell wall curvatures)[43−46]

$$\Delta E_{tot} = \Delta E_{ad} + \Delta E_{str} + \Delta E_c \quad (1)$$

The bending energy change (ΔE_c) was not considered in this study because the ΔE_c value was found to be negligible compared to ΔE_{ad} (see Supporting Information Section 2).[45] Upon contact with a substratum, if $\Delta E_{tot} > 0$, it is energetically unfavorable for the cell to adhere on the surface, whereas if $\Delta E_{tot} < 0$, it is energetically favorable for the cell to attach. The lower the total energy in the adherent state (relative to the planktonic state), the higher the probability of a cell remaining adherent on the surface.

Nonspecific interactions (e.g., van der Waals, electrostatic, and acid−base interactions) between the cell wall and the substratum govern the early-stage cell adhesion on abiotic surfaces,[42] thus specific adhesion (e.g., by adhesins[47]) is ignored in this model. ΔE_{ad} is defined as the surface integral of the work of adhesion (w_{ad}) over the cell−substratum contact area (A_{ad})

$$\Delta E_{ad} = -\oint w_{ad}\, dA_{ad} \quad (2)$$

Assuming homogeneous cell surface conditions, eq 2 is simplified to

$$\Delta E_{ad} = -w_{ad} A_{ad} \quad (3)$$

The value of w_{ad} is determined through experimental measurement of the dispersive (γ^d_{cell}, γ^d_s) and polar (γ^p_{cell}, γ^p_s) components of the surface energies of the *C. albicans* yeast (denoted with subscript cell) and the solid substratum (denoted with subscript s) in conjunction with the equation below[48,49]

$$w_{ad} = 2\sqrt{\gamma^d_{cell}\gamma^d_s} + 2\sqrt{\gamma^p_{cell}\gamma^p_s} \quad (4)$$

An increase in the cell−substratum contact area (A_{ad}) coincides with a stretching of the cell wall and a corresponding change in the stretching energy, ΔE_{str}, that can be calculated from the following equation[50]

$$\Delta E_{str} = \frac{1}{2} k_{str} \frac{(A - A_0)^2}{A_0} \quad (5)$$

where k_{str} is the stretching modulus, A is the total surface area of the stretched cell after adhesion, and A_0 is the original cell surface area in

DOI: 10.1021/acsami.8b02907
ACS Appl. Mater. Interfaces 2018, 10, 15477−15486

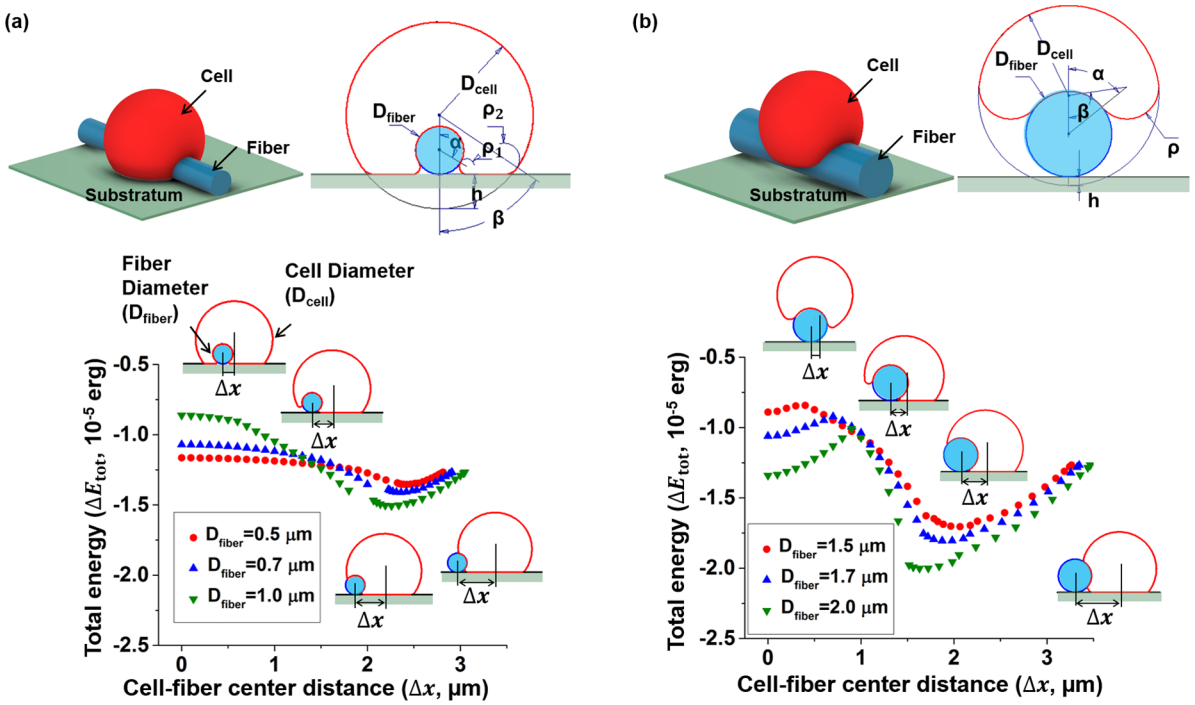

Figure 1. Relative total energy (ΔE_{tot}) of a *C. albicans* yeast cell interacting with a single fiber vs cell−fiber center distance (Δx) for (a) 0.5−1.0 μm ($D_{fiber} \leq D_{crit}$) and (b) 1.5−2.0 μm ($D_{fiber} > D_{crit}$). In this case, w_{ad} = 77 mJ/m^2, k_{str} = 416 mN/m, and D_{crit} = 1.2 μm. The cartoons show cell shape (and relevant geometrical parameters) in the cases of $D_{fiber} \leq D_{crit}$ and $D_{fiber} > D_{crit}$. Fibers are shown in blue and cells are outlined in red. For comparison ΔE_{tot}(unmodified) = -1.3×10^{-5} erg.

the planktonic state, which can be approximated as a sphere with the diameter of D_{cell}.

The stretching modulus was calculated from the following equation[51,52]

$$k_{str} = Yh \tag{6}$$

where Y is the average Young's modulus of the cell wall and h is the average cell wall thickness.

The relative total energy of the adherent cell can then be simplified as

$$\Delta E_{tot} = \Delta E_{ad} + \Delta E_{str} = -w_{ad}A_{ad} + \frac{1}{2}k_{str}\frac{(A - A_0)^2}{A_0}$$
$$= -(2\sqrt{\gamma_{cell}^{d}\gamma_{s}^{d}} + 2\sqrt{\gamma_{cell}^{p}\gamma_{s}^{p}})A_{ad} + \frac{1}{2}Yh\frac{(A - A_0)^2}{A_0} \tag{7}$$

The unknown parameters in eq 7 are A_{ad} and A. On the basis of the experimental observations, we assume that the overall cell shape remains spherical and any deformation is localized to the regions of interaction with the underlying substratum. Volume change was considered negligible due to presence of a cell wall in *C. albicans* and lack of significant change in osmotic pressure.[53] For each cell centroid−fiber centerline separation distance (Δx, shown in Figure 1), with the aforementioned shape and volume constraints, we calculated ΔE_{tot} for every combination of the geometric parameters (Figure 1 and Supporting Information Section 3) in a physically meaningful range (e.g., $0 < \alpha < \pi$, $0 < \beta < \pi$, $\rho > 0$). The geometry of the cell that yielded the minimum ΔE_{tot} was computed using an optimization routine (see Supporting Information for computational details).

2.2. Nanofiber Deposition. A 0.125 mm polystyrene (PS) sheet (Goodfellow Cambridge Ltd., Huntington, U.K.) was cut into 3 mm × 15 mm rectangular pieces. The PS substrata were washed with 100% ethanol, rinsed with deionized (DI) water, and air-dried. PS fibers with uniform diameters (D_{fiber} = 0.5−2.0 μm, Figure S2) at edge-to-edge spacing of 2.0 μm were deposited onto PS substrata using the nonelectrospinning Spinneret-based Tunable Engineered Parameters (STEP) technique.[54−56] Briefly, PS (molecular weight: 2×10^6 g/mol, Scientific Polymer Products, Ontario, NY) dissolved in xylene was pumped through a glass micropipette to form a droplet. A continuous fiber was extruded from the polymer solution droplet at the tip of the micropipette, and was deposited onto a rotating polystyrene substratum, which was mounted onto a stepper motor attached to a motorized *XYZ* positioning stage. The rotational speed of the motor and the translational speed of the stage determined the edge-to-edge spacing between the fibers. The diameter was controlled by changing the diameter of the micropipette and the concentration of the polymer in the PS−xylene solution. The polystyrene was dissolved in xylene at 14−25% by weight to achieve fiber diameters in the range of 500−2000 nm. To maintain the 2.0 μm spacing across different diameter samples, the linear velocity of the motorized stage was varied when spinning each of the diameters. For the catheter experiments, latex (Bard Medical, Covington, GA) and silicone (Rochester Medical, Stewartville, MN) urinary catheters and polyurethane (PU) dog femoral central vein catheter (SAI Infusion Technologies, Lake Villa, IL) were cut to 15 mm long pieces and were used as substrata on which 1.0−1.2 μm diameter fibers were deposited at the edge-to-edge separation distance of 2.0 μm. Prior to all experiments, the diameter and separation distances of the fibers were analyzed using an environmental scanning electron microscope (ESEM, FEI Quanta 600 FEG, Hillsboro, OR) in low vacuum mode. Ten random areas (magnification: 8000×) along the horizontal centerline of the fibrous samples were imaged. Measurements of the diameter and separation distances were done using the image analysis software ImageJ.

2.3. Cell Culture. *C. albicans* was selected due to its prevalence in urinary tract infection.[41,57] Wild-type *C. albicans* strain SC5314[58] (ATCC MYA2876, American Type Culture Collection, Manassas, VA) was grown on a Sabouraud dextrose agar (SDA) plate at 37 °C for 24 h. Several (3−5) colonies from the plate were inoculated into 10 mL of yeast nitrogen base with 50 mM dextrose (YNBD) medium, and the suspension was shaken at 37 °C and 150 rpm for 24 h.

2.4. Dynamic Retention Assay. All retention assays were performed in a Center for Disease Control (CDC) biofilm reactor (model CBR-90-2, Figure S3) according to the previously established methods.[59,60] Prior to all experiments, the nanofiber-coated substrata

DOI: 10.1021/acsami.8b02907
ACS Appl. Mater. Interfaces 2018, 10, 15477−15486

Table 1. Contact Angles (θ), Surface Energies (γ^d, γ^p, and γ), and Work of Adhesion (w_{ad}) of Yeast, PS Substratum, PS Fiber Material, PU Catheter, Latex Catheter, and Silicone Catheter

	contact angle (θ, deg)						
	water	formamide	diiodomethane	γ^d (mJ/m^2)	γ^p (mJ/m^2)	γ (mJ/m^2)	w_{ad} with yeast (mJ/m^2)
C. albicans yeast	56.4 ± 7.9	59.5 ± 8.4	37.4 ± 6.8	28.3 ± 6.9	17.8 ± 5.4	46.1 ± 8.8	
PS substratum	88.8 ± 1.0	60.9 ± 1.4	22.9 ± 1.9	44.0 ± 2.0	0.6 ± 0.2	44.6 ± 2.0	77.3
PS fiber material	82.7 ± 0.6	66.7 ± 2.3	26.0 ± 1.5	37.5 ± 4.4	2.4 ± 1.1	39.9 ± 4.5	78.3
PU catheter	82.3 ± 0.2	64.0 ± 3.7	80.3 ± 1.8	15.1 ± 1.3	11.3 ± 1.1	26.4 ± 1.7	69.7
latex catheter	110 ± 3	89.2 ± 0.5	90.0 ± 0.6	13.2 ± 1.0	1.1 ± 0.3	14.3 ± 1.0	47.5
silicone catheter	113 ± 2	104 ± 1	90.4 ± 0.8	10.3 ± 0.8	0.9 ± 0.2	11.2 ± 0.8	42.1

were sterilized under ultraviolet light inside a biological safety cabinet for 45 min and were conditioned by soaking in fetal bovine serum overnight at 37 °C. The substrata were then mounted onto the bioreactor rods. Each rod held triplicate samples of the same fiber diameter. *C. albicans* culture, grown in YNBD at 37 °C and 150 rpm for 24 h, was diluted to OD_{520} = 0.385 (~1 × 10^7 CFU/mL) in YNBD medium. Subsequently, 8 mL of the diluted culture and 392 mL of YNBD medium were mixed and added to the CDC biofilm reactor. The bioreactor was placed on a magnetic stir plate inside an incubator at 80 rpm and 37 °C for 24 h. To determine the number of viable cells on each sample, the bioreactor rods were carefully taken out and the substrata were removed using a pair of fine tipped tweezers. The substrata were then each rinsed and placed inside 15 mL polypropylene test tubes, containing 10 mL of Sabouraud dextrose broth (SDB). The cells adhered to the samples were removed by consecutive sonication (42 kHz, 70 W) and vortex mixing at 1000 rpm, for 30 s each, repeated three times. The resulting cell suspension was serially diluted in SDB, and a 100 μL aliquot from the final dilution was spread on SDA plates using sterile cell spreaders. The plates were incubated at 37 °C for 24 h, and the number of colonies was counted. The colony counts from the nanofiber-coated substrata were compared to the unmodified (control) substrata from the same experiment by taking the ratio of the number of cells on the nanofiber-coated surface of each diameter and dividing it by the number of cells on the surface of the unmodified substratum from the same experiment. This makes the ratio on unmodified surface equal to 1, anything below 1 indicated a decrease in the adhesion of cells (relative to the control), and anything above indicates an increase.

2.5. Scanning Electron Microscopy. After the 24 h experiment in the bioreactor, selected samples were gently washed in phosphate-buffered saline (PBS) and then placed in 2.5% glutaraldehyde in PBS for 2 h at 4 °C. Subsequently, the samples were soaked in PBS for 20 min twice and then in DI water for 20 min twice. The samples were then serially dehydrated by soaking in 35, 50, 75, and 95% ethanol for 30 min each and in 100% ethanol for 3 × 30 min. The 100% ethanol was pipetted out, and the samples were air-dried overnight. The air-dried samples were gold coated prior to scanning electron microscopy (SEM) imaging.

2.6. Contact Angle Measurement and Surface Energy Calculation. Contact angle measurements were performed to estimate the surface energy of *C. albicans* yeast.[61] After 24 h of growth, the yeast culture was harvested, washed twice by centrifugation, and suspended in DI water. The yeast cells were then collected on a nitrocellulose membrane filter (0.22 μm pores, Millipore) to a density of 10^8 cells/mm^2 to form a dense yeast film. The filters were placed on a microscope glass slide with double-side tape and dried in a desiccator until stable contact angles can be measured.[37] Contact angles of two polar liquids (DI water, formamide) and one apolar liquid (diiodomethane) were measured by depositing only one liquid droplet in the center of each yeast film. Time-lapse images at 1 frame/s were recorded upon the deposition of the liquid droplet. The contact angles were measured using the images that depicted the initial placement of each drop on the yeast film. A minimum of three independent measurements were conducted for each probe liquid.

Contact angle measurements were also performed to determine the surface energy of the PS substratum material and PS material used in fiber manufacturing. The PS substratum was cut to 10 mm × 10 mm pieces, and the PS fiber material was solution cast on a microscope glass slide to a final thickness of 100 μm. The PS substratum and the cast PS thin film were cleaned with ethanol and DI water and air-dried overnight prior to contact angle measurements. Contact angles of DI water, formamide, and diiodomethane on the PS substratum and cast PS thin film were measured by depositing one liquid drop at the center of each substratum. A minimum of three independent measurements were conducted for each substratum and each probe liquid.

A glass cuvette was treated by hexamethyldisilazane vapor to ensure a hydrophobic surface. The glass cuvette was filled with DI water, formamide, or diiodomethane. The latex and silicone urinary catheters and the PU central vein catheter were cut to 10 mm long pieces and rinsed with ethanol and DI water and dried overnight. The catheter pieces were vertically inserted into the liquid, and the contact angles between the liquid and the catheter walls were measured. A minimum of three independent measurements were conducted for each catheter type and each probe liquid.

The solid–liquid (γ_{SL}) surface energy, the solid–vapor (γ_{SV}) surface energy, and the dispersive and polar components of the solid surface energy (γ_S^d and γ_S^p, respectively) can be determined from the measured contact angle (θ) and the known values of the dispersive (γ_L^d) and polar (γ_L^p) components of the probe liquid surface energy (γ_{LV}), using eqs 8 through 11

$$\gamma_{SL} = \gamma_{SV} + \gamma_{LV} - 2(\gamma_S^d\gamma_L^d)^{1/2} - 2(\gamma_S^p\gamma_L^p)^{1/2} \quad (8)$$

$$\gamma_{SV} = \gamma_{SL} + \gamma_{LV}\cos\theta \quad (9)$$

$$\gamma_{SV} = \gamma_S^d + \gamma_S^p \quad (10)$$

$$\gamma_{LV} = \gamma_L^d + \gamma_L^p \quad (11)$$

In practice, this is accomplished by combining the preceding equations to fit the slope–intercept form of the equation of a line[48]

$$\gamma_{LV}(1+\cos\theta)/2(\gamma_L^d)^{1/2} = (\gamma_S^p)^{1/2}(\gamma_L^p/\gamma_L^d)^{1/2} + (\gamma_S^d)^{1/2} \quad (12)$$

With the left side of eq 12 plotted against $(\gamma_L^p/\gamma_L^d)^{1/2}$, the slope is $(\gamma_S^p)^{1/2}$ and the intercept is $(\gamma_S^d)^{1/2}$. For each solid surface, we analyzed the contact angle measurement results for each of the three probe liquids and plotted a best-fit line through the data to determine the slope and intercept and hence the dispersive (γ_S^d) and polar components (γ_S^p) of the solid surface energy.

2.7. Statistical Analysis. The one-way analysis of variance (ANOVA) and Fisher's least significant difference test were conducted for statistical analysis. All analyses were conducted using Origin 9.0 (OriginLab, Northampton, MA). To determine the statistical significance, the threshold for the p value was set at 0.05. The error bars for all experimental data represent the standard deviations.

3. RESULTS

3.1. Biophysical Modeling Results. We first analyzed the simplest case, wherein a cell only interacts with one PS fiber on a PS substratum. As shown in Figure 1, the relative total energy of the cell, ΔE_{tot}, varies with fiber diameter, D_{fiber}, as well as

DOI: 10.1021/acsami.8b02907
ACS Appl. Mater. Interfaces 2018, 10, 15477–15486

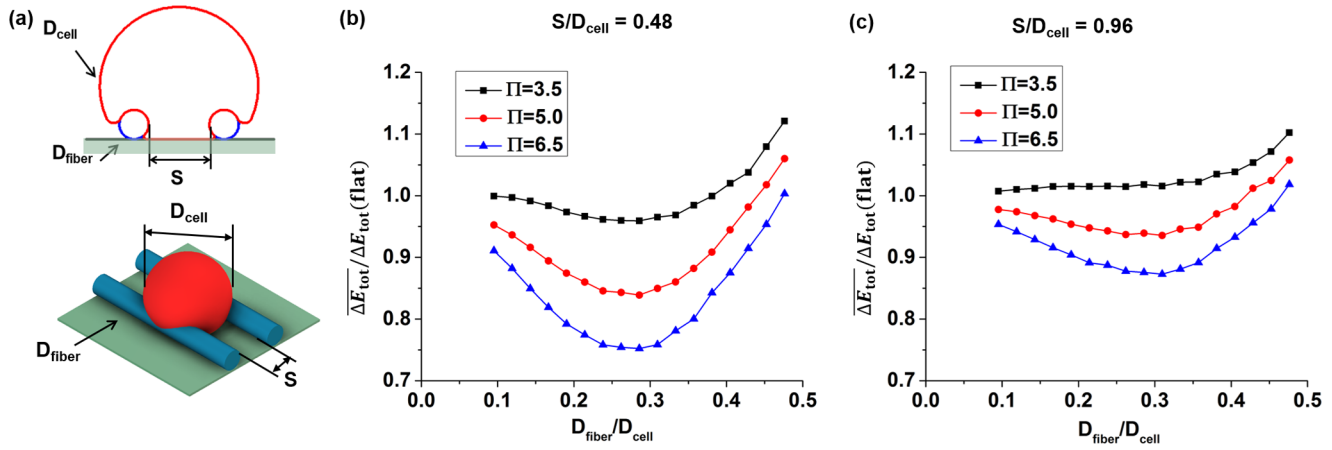

Figure 2. (a) Schematics of a *C. albicans* yeast cell on a nanofiber-coated substratum. Fibers are outlined in blue and the cell is outlined in red. (b) Normalized spatially averaged total energy ($\overline{\Delta E_{tot}}/\Delta E_{tot}$(unmodified)) of a *C. albicans* yeast cell on nanofiber-coated substrata vs normalized fiber diameter (D_{fiber}/D_{cell}) for Π = 3.5, 5.0, and 6.5, and normalized edge-to-edge fiber spacing of S/D_{cell} = 0.48 and (c) S/D_{cell} = 0.96.

location of the cell centroid with respect to the fiber centerline, denoted as Δx. From microscopy images of planktonic *C. albicans* yeast cells, the average diameter of the cell, D_{cell}, was measured to be 4.2 ± 1.2 μm (N = 235). For Δx = 0, when the cell is adhered to a fiber with diameter smaller than that of the critical fiber diameter, D_{crit}, the cell can wrap around the fiber and contact the underlying substratum (Figure 1a). However, when adhered to a fiber with diameter larger than D_{crit}, the cell will not contact the underlying substratum (Figure 1b). The magnitude of D_{crit} depends on the properties of the cell and the substratum. Young's modulus of *C. albicans* yeast cell was taken to be 1.6 MPa and the average cell wall thickness was taken to be 260 nm, as previously reported in the literature.[62,63] Using these values, the stretching modulus of the cell, k_{str}, was determined from eq 6 to be 416 mN/m. Work of adhesion (w_{ad}) between the yeast cell and PS was calculated from eq 4 to be w_{ad} = 77.3 mJ/m^2 for interaction with the PS substratum and w_{ad} = 78.3 mJ/m^2 for interaction with the PS fiber (Table 1). For the aforementioned k_{str} and w_{ad} values, D_{crit} was determined to be 1.2 μm. For the case $D_{fiber} \leq D_{crit}$, ΔE_{tot} has only one minimum, which is a function of fiber diameter and occurs in the range of Δx = 2.2−2.4 μm (Figure 1a). For $D_{fiber} > D_{crit}$, ΔE_{tot} has two local minima, one at Δx = 0 and the other is a function of fiber diameter and occurs at Δx = 1.6−2.1 μm (Figure 1b).

After analyzing the case of a cell interacting with a single fiber, the model was extended to a cell interacting with two fibers when the fiber edge-to-edge spacing (S) is smaller than the cell diameter (D_{cell}). ΔE_{tot} of one cell interacting with two fibers was calculated from ΔE_{tot} of a cell interacting with each of the two fibers separately, with the assumption that cell deformation caused by a fiber is confined to the vicinity of the fiber and is much smaller than the overall cell surface area change (see Supporting Information Section 3.4). For a given fiber diameter and spacing, ΔE_{tot} of the cell varies with its location relative to the fibers. We define the spatially averaged ΔE_{tot} (denoted as $\overline{\Delta E_{tot}}$) as the average total energy of an adherent cell over all possible cell−fiber distance values for the patterned surface. Each patterned surface (with nanofiber coating of a particular diameter and a particular separation distance) is represented by its corresponding $\overline{\Delta E_{tot}}$. We assume that the possibility of a cell initially contacting the patterned substratum is equal in every location, so $\overline{\Delta E_{tot}}$ is calculated as (see Supporting Information Section 3.5)

$$\overline{\Delta E_{tot}} = \frac{1}{N}\sum_{i=1}^{N} \Delta E_{tot}(i) \tag{13}$$

for a sufficiently large number, N, of equal area increments, where $\Delta E_{tot}(i)$ is the total energy of the cell adherent to the patterned surface at a position with the distance of the cell centroid and one fiber centerline of $\Delta x(i)$, for $0 \leq \Delta x(i) \leq S + D_{fiber}$ (see Figure S3.8).

The nondimensionalized results of the analysis are shown in Figure 2. To generalize the results to different cell sizes, we normalized the fiber diameter and spacing to the cell diameter (i.e., D_{fiber}/D_{cell}, S/D_{cell}). Furthermore, a new nondimensional parameter Π was introduced to represent ratio of the stretching modulus (a measure of the cell wall stiffness) to the work of adhesion (a measure of the interaction between the cell wall and the substratum).

$$\Pi = k_{str}/w_{ad} \tag{14}$$

We then quantified the effect of nanofiber coating diameter and spacing on the spatially averaged total energy of the cell attached on nanofiber-coated substrata and normalized it by the total energy of the cell adhered on the unmodified substratum ($\overline{\Delta E_{tot}}/\Delta E_{tot}$(unmodified)). A value of $\overline{\Delta E_{tot}}/\Delta E_{tot}$(unmodified) < 1 indicates that, on average, the cell on the patterned surface had a less negative value for ΔE_{tot} than does on an unmodified surface and thus the patterned surface is less favorable for adhesion. This assertion is consistent with earlier reports on the influence of surface energy modification on bacterial adhesion. For instance, Liu et al. showed that the number of cell colonies attached to the surface decreased with increasing the total interaction energy.[64] As shown in Figure 2, the spatially averaged normalized total energy has one minimum value. For instance, when Π = 5.0 and S/D_{cell} = 0.48, the spatially averaged normalized total energy reaches its minimum value at D_{fiber}/D_{cell} = 0.29. In this case, the magnitude of the ΔE_{tot} is 15% less than the ΔE_{tot}(unmodified); thus, this nanofiber-coated surface is less favorable for adhesion, compared with the unmodified surface. For a given range of D_{fiber}/D_{cell}, the curvature at the minimum point is a strong function of the Π value but it also depends on S/D_{cell}. For a

DOI: 10.1021/acsami.8b02907
ACS Appl. Mater. Interfaces 2018, 10, 15477−15486

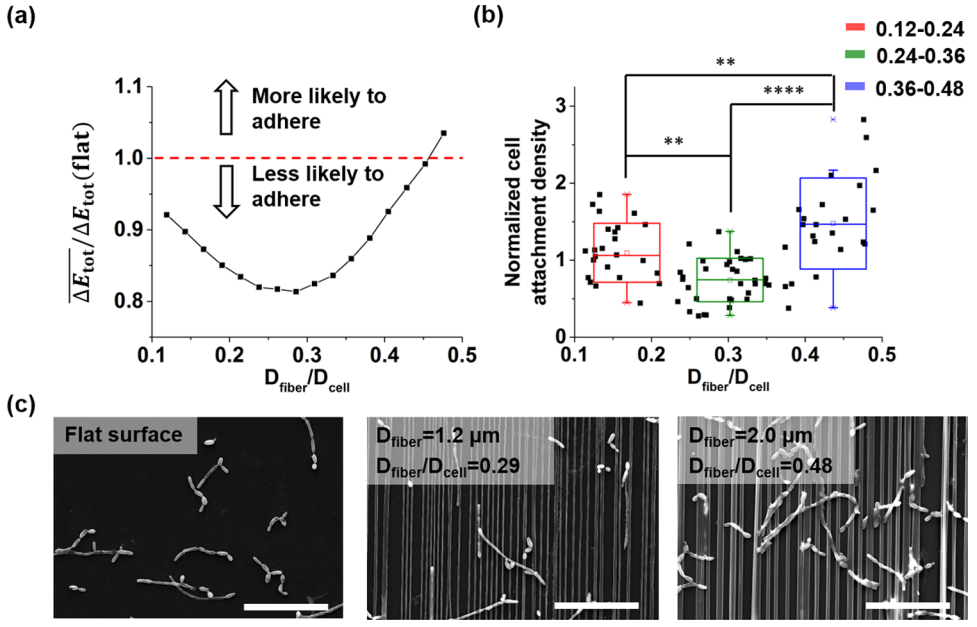

Figure 3. (a) $\overline{\Delta E_{tot}}/\Delta E_{tot}$(unmodified) vs D_{fiber}/D_{cell} for fiber edge-to-edge spacing of 2.0 μm (S/D_{cell} = 0.48). (b) Normalized cell attachment density (relative to the attachment density on the unmodified substratum) vs D_{fiber}/D_{cell} at S/D_{cell} =0.48 (N = 80). Comparison of normalized cell attachment density for fiber groups of D_{fiber}/D_{cell} = 0.12−0.24, 0.24−0.36, and 0.36−0.48; ****p value < 0.0001, **p value < 0.01. (c) SEM images of *C. albicans* on unmodified D_{fiber} = 1.2 μm and D_{fiber} = 2.0 μm fiber-coated substrata. All scale bars are 50 μm.

fixed S/D_{cell}, the normalized total energy is more sensitive to changes of D_{fiber}/D_{cell} at higher Π values. A higher Π value physically represents either a stiffer cell wall (higher k_{str}) or a lower cell−substratum adhesion strength (lower w_{ad}). This indicates that stiffer cells or cells with weaker adhesion are more sensitive to changes in the surface feature size (i.e., fiber diameter). For a fixed Π, the change of the normalized total energy is more significant at a smaller S/D_{cell} because the nanofiber density (number of nanofibers per unit surface area) is higher in this case.

3.2. Experimental Validation with PS Nanofiber-Coated PS Substrata. As shown in Table 1, contact angles of the *C. albicans* yeast film, PS substratum, and PS fiber material with water, formamide, and diiodomethane were measured. From the contact angle measurements and eq 12, surface energy (γ) values and their corresponding dispersive (γ^d) and polar (γ^p) components were calculated. Work of adhesion (w_{ad}) between the yeast cell and the relevant material was calculated from eq 4.

Using the calculated w_{ad} for PS substratum and k_{str} = 416 mN/m values, Π is calculated to be 5.4. For this Π value and a fiber spacing of S = 2 μm (S/D_{cell} = 0.48), the normalized total energy has a minimum value at D_{fiber}/D_{cell} = 0.29 (Figure 3a), suggesting an optimal fiber diameter of 1.2 μm for minimizing *C. albicans* adhesion.

To examine the relation between the single-cell total free energy (Figure 3a) and population-scale cell attachment density, we next conducted a dynamic retention assay on fiber-coated substrata where the fiber spacing was fixed at S/D_{cell} = 0.48 and the D_{fiber}/D_{cell} was varied in the range of 0.12−0.48. The cell attachment density on fiber-coated surfaces was normalized to the cell attachment density on the unmodified surface and plotted against D_{fiber}/D_{cell} (Figure 3b). The fiber diameters were divided into three different groups (D_{fiber}/D_{cell} = 0.12−0.24, 0.24−0.36, and 0.36−0.48), and the normalized cell attachment densities were averaged in each group. The average normalized cell attachment density for the three groups are 1.09 ± 0.38 (N = 26), 0.74 ± 0.28 (N = 31), and 1.47 ± 0.59 (N = 23), respectively. A one-way ANOVA test demonstrated significant differences between the groups (Figure 3b). The SEM images of the substrata (shown in Figure 3c) after the experiment displayed the difference in cell attachment density between the unmodified surface, 1.2 μm fiber-coated surface (D_{fiber}/D_{cell} = 0.29), and 2.0 μm fiber-coated surface (D_{fiber}/D_{cell} = 0.48). The experimental results confirmed our hypothesis that the total free energy of a single adherent cell on a patterned surface is indicative of the microbial attachment density on the surface. Furthermore, it reaffirmed the model's predicted behavior that only a specific range of fiber diameters could reduce the cell attachment density, whereas other fiber diameters increased it. This is because when the fiber diameters are either too small or too large, the cell's total energy decreases as it utilizes the fiber to increase the adhesion area (reduce ΔE_{ad}) with minimal stretching (no significant increase in ΔE_{str}, Figure S4).

3.3. Experimental Validation with PS Nanofiber-Coated Catheters. To further investigate the practical applicability of our biophysical model, the effect of PS nanofiber coating on the density of cell attachment to the catheters was explored. Commercially available latex and silicone urinary catheters and PU femoral central vein catheter were used in this study. Contact angles of these catheter materials with water, formamide, and diiodomethane were first measured (Table 1). From these contact angle measurements, γ^d, γ^p, and γ were calculated using eq 12. The values for the work of adhesion, w_{ad}, between the yeast cell and the PU and latex and silicone catheters were calculated to be 69.7, 47.5, and 42.1 mJ/m^2, respectively. As described in the previous section, w_{ad} between the yeast cell and the PS fiber material is 78.3 mJ/m^2 and k_{str} of the cell wall is 416 mN/m. The simulation results for the spatially averaged normalized total energy ($\overline{\Delta E_{tot}}/\Delta E_{tot}$(unmodified)) against the nondimensional fiber

DOI: 10.1021/acsami.8b02907
ACS Appl. Mater. Interfaces 2018, 10, 15477−15486

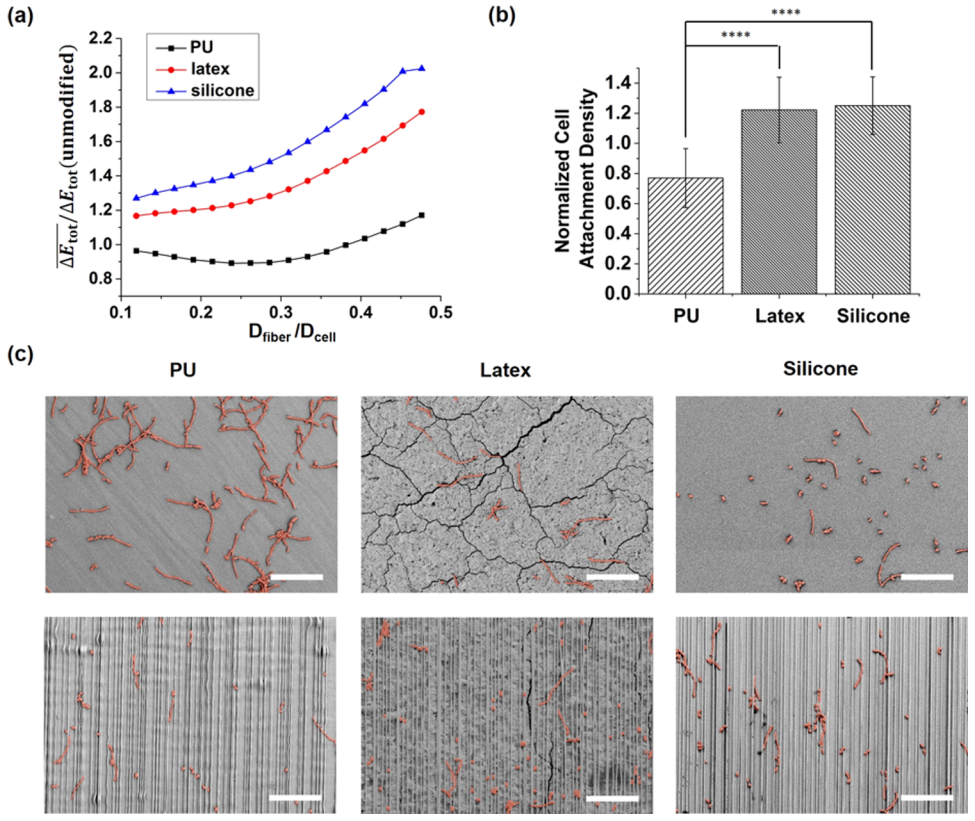

Figure 4. (a) Simulation results for $\overline{\Delta E_{tot}}/\Delta E_{tot}$(unmodified) vs D_{fiber}/D_{cell} for PU and latex and silicone catheters coated with PS nanofibers at S/D_{cell} = 0.48. (b) Normalized cell attachment density for PU and latex and silicone catheters coated with 1.0−1.2 μm fibers (D_{fiber}/D_{cell} = 0.24−0.29 and S/D_{cell} = 0.48), N = 12, 10, and 11, respectively, ****p value < 0.0001. (c) SEM images of *C. albicans* on unmodified and nanofiber-patterned catheters. All scale bars are 50 μm.

diameter (D_{fiber}/D_{cell}) at S/D_{cell} = 0.48 for the PU and latex and silicone catheters coated with PS fibers are shown in Figure 4a. Only the PU catheter has a region of D_{fiber}/D_{cell} values that results in a total energy that is less favorable for adhesion, compared with the unmodified PU catheter ($\overline{\Delta E_{tot}}/\Delta E_{tot}$(unmodified) < 1). On the other hand, both the treated latex and silicone catheters have total energy values that are more favorable for adhesion with the deposited PS nanofibers for all D_{fiber}/D_{cell}. This is because w_{ad} for the PS fiber (78.3 mJ/m^2) is closer to w_{ad} for the PU (69.7 mJ/m^2) catheter but much higher than that of the latex (47.5 mJ/m^2) and silicone (42.1 mJ/m^2) catheters. As a result, only for the PS nanofiber-coated PU catheter in the range of D_{fiber}/D_{cell} = 0.12−0.38, the change in the stretching energy due to the surface patterns dominated the higher w_{ad} and yielded $\overline{\Delta E_{tot}}/\Delta E_{tot}$(unmodified) < 1. There is a minimum for the spatially averaged normalized total energy in the D_{fiber}/D_{cell} region of 0.24−0.29, which corresponds to fiber diameters of 1.0−1.2 μm.

To experimentally validate the model predictions, PS fibers with diameters of 1.0−1.2 μm (D_{fiber}/D_{cell} = 0.24−0.29) were deposited on the PU and latex and silicone catheter surfaces using the STEP technique and a dynamic retention assay was conducted for unmodified and nanofiber-coated catheters. As shown in Figure 4b, the cell attachment density normalized by the respective unmodified surface attachment density is 0.77 ± 0.20 for the PU catheter, 1.22 ± 0.22 for the latex catheter, and 1.25 ± 0.19 for the silicone catheter. Thus, the experimental results are in agreement with the predictions from the model. Combined together, our findings show that deposition of PS fibers is only effective in mitigating cell attachment on the PU catheter; however, introducing PS nanofibers onto the latex and silicone catheters increases the cell attachment density because the introduction of fibers increases the work of adhesion between the cell and the substratum. The SEM images in Figure 4c show the cell attachment density in the presence and absence of the fiber coating on the different catheters.

4. DISCUSSION

The biophysical model developed herein utilizes a description of the total energy (adhesion energy and stretching energy) of a single adherent *C. albicans* yeast cell to predict the effect of nanofiber coating on the cell attachment density. Results from the model show that for a given cell size and biophysical properties, patterning a surface with nanofibers can increase or decrease the cell attachment density, depending on the substratum and fiber materials as well as the fiber diameter and spacing. For example, depositing fibers made of a material that causes a significant increase in w_{ad} (decrease in ΔE_{ad}) will lead to a reduced total energy of the adherent cell and increased cell attachment density (e.g., depositing PS fibers on latex or silicone catheters, as shown in Figure 4b). Even when depositing fibers of the same material as the substratum (e.g., depositing PS fibers on PS substratum), not all fiber diameters will increase the total energy and mitigate cell attachment (Figure 3). In the application of depositing nanofibers on catheter surfaces, if the fiber material is the same as the catheter material (e.g., depositing PU fibers on the PU catheter), the

DOI: 10.1021/acsami.8b02907
ACS Appl. Mater. Interfaces 2018, 10, 15477−15486

effect of the pattern geometry will be more pronounced (Figure 5). As shown in Figure 2, the normalized total energy is more

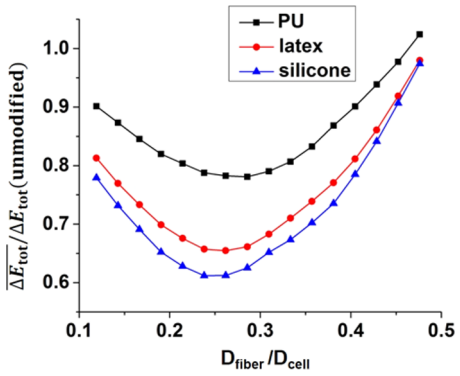

Figure 5. Simulation result of $\overline{\Delta E_{tot}}/\Delta E_{tot}$(unmodified) vs D_{fiber}/D_{cell} for PU and latex and silicone catheters coated with nanofibers of the same material at a spacing of S/D_{cell} = 0.48.

sensitive to changes of D_{fiber}/D_{cell} at higher Π values. Silicone has the lowest w_{ad} (Table 1) and therefore the highest Π value ($\Pi = k_{str}/w_{ad}$ = 9.9). As a result, the minimum normalized total energy for silicone is the lowest (i.e., $\overline{\Delta E_{tot}}/\Delta E_{tot}$(unmodified) = 0.61 at D_{fiber}/D_{cell} = 0.24–0.26 for S/D_{cell} = 0.48). When designing nanostructure-modified surfaces, the surface energy of the material comprising the nanostructures should be as low as possible. For a given coating material, our biophysical model can predict the optimal feature size (e.g., nanofiber diameter) and configuration (fiber spacing) that would minimize $\overline{\Delta E_{tot}}/\Delta E_{tot}$(unmodified) to ensure the best antiadhesion effect. This biophysical model can be extended to other nanostructures with development of appropriate geometrical relations (similar to those developed in the Supporting Information Section 3). Furthermore, because this model is generalized through the use of nondimensional parameters, it can be applied to other microorganisms and substrata with experimentally measured k_{str}, w_{ad}, and surface energy values.

5. CONCLUSIONS

We have developed and experimentally validated a biophysical model for the adhesion of the model fungal pathogen, *C. albicans*, on nanofiber-coated surfaces and quantified the total energy (adhesion energy and stretching energy) of the adherent cell as a function of the geometry (i.e., diameter) and configuration (i.e., spacing) of the nanofibers. A dynamic retention assay of *C. albicans* on PS fiber-coated PS substrata was conducted to validate our hypothesis that the adherent cell total energy trend is predictive of the cell attachment density trend. We show that the surface pattern design that yielded the highest total energy, results in the lowest cell attachment density. Guided by our biophysical model, we patterned PU and latex and silicone catheters with PS fibers and demonstrated good agreement between the model and the experiment. This biophysical model in conjunction with the nondimensional parameters developed in this study can be extended to other nanostructures, microorganisms, and substratum materials for efficient ab initio biomaterial design, either to decrease pathogenic microbial adhesion density or increase beneficial microbial adhesion density.

ASSOCIATED CONTENT

Supporting Information

The Supporting Information is available free of charge on the ACS Publications website at DOI: 10.1021/acsami.8b02907.

Mathematical derivations and expanded discussions of the biophysical model and experimental methods (PDF)

AUTHOR INFORMATION

Corresponding Author

*E-mail: behkam@vt.edu.

ORCID

Zhou Ye: 0000-0003-4220-0919

Amrinder S. Nain: 0000-0002-9757-2341

Bahareh Behkam: 0000-0002-2174-2914

Author Contributions

⊥Z.Y. and A.K. contributed equally to this work.

Notes

The authors declare no competing financial interest.

ACKNOWLEDGMENTS

This work was in part supported by the Institute for Critical Technology and Applied Science (ICTAS) at Virginia Tech and the Thomas F. and Kate Miller Jeffress Memorial Trust. Z.Y. acknowledges financial support from the Robert E. Hord, Jr., Mechanical Engineering Graduate Fellowship. A.K. acknowledges financial support from AMA Adhesion and Sealant Undergraduate Student Award. We extend our gratitude to Professor David Dillard for insightful discussions and Steve McCartney for assistance with environmental scanning electron microscopy. We would also like to thank our colleague Emir Sahmanovic for the help with the preliminary experiments.

REFERENCES

(1) Costerton, J. W.; Stewart, P. S.; Greenberg, E. P. Bacterial Biofilms: A Common Cause of Persistent Infections. *Science* **1999**, *284*, 1318–1322.

(2) Mah, T. F. C.; O'Toole, G. A. Mechanisms of Biofilm Resistance to Antimicrobial Agents. *Trends Microbiol.* **2001**, 34–39.

(3) Kumar, C. G.; Anand, S. K. Significance of Microbial Biofilms in Food Industry: A Review. *Int. J. Food Microbiol.* **1998**, *42*, 9–27.

(4) Meng, F.; Chae, S.-R.; Drews, A.; Kraume, M.; Shin, H.-S.; Yang, F. Recent Advances in Membrane Bioreactors (MBRs): Membrane Fouling and Membrane Material. *Water Res.* **2009**, *43*, 1489–1512.

(5) Simões, M.; Simões, L. C.; Vieira, M. J. A Review of Current and Emergent Biofilm Control Strategies. *LWT–Food Sci. Technol.* **2010**, *43*, 573–583.

(6) Beech, I. B.; Sunner, J. Biocorrosion: Towards Understanding Interactions between Biofilms and Metals. *Curr. Opin. Biotechnol.* **2004**, *15*, 181–186.

(7) Francolini, I.; Donelli, G. Prevention and Control of Biofilm-Based Medical-Device-Related Infections. *FEMS Immunol. Med. Microbiol.* **2010**, *59*, 227–238.

(8) Donlan, R. M.; Costerton, J. W. Biofilms: Survival Mechanisms of Clinically Relevant Microorganisms. *Clin. Microbiol. Rev.* **2002**, *15*, 167–193.

(9) Marchetti, A.; Rossiter, R. Economic Burden of Healthcare-Associated Infection in US Acute Care Hospitals: Societal Perspective. *J. Med. Econ.* **2013**, *16*, 1399–1404.

(10) Banerjee, I.; Pangule, R. C.; Kane, R. S. Antifouling Coatings: Recent Developments in the Design of Surfaces That Prevent Fouling by Proteins, Bacteria, and Marine Organisms. *Adv. Mater.* **2011**, *23*, 690–718.

DOI: 10.1021/acsami.8b02907
ACS Appl. Mater. Interfaces 2018, 10, 15477–15486

(11) Hochbaum, A. I.; Aizenberg, J. Bacteria Pattern Spontaneously on Periodic Nanostructure Arrays. *Nano Lett.* **2010**, *10*, 3717−3721.
(12) Chung, K. K.; Schumacher, J. F.; Sampson, E. M.; Burne, R. A.; Antonelli, P. J.; Brennan, A. B. Impact of Engineered Surface Microtopography on Biofilm Formation of *Staphylococcus aureus*. *Biointerphases* **2007**, *2*, 89−94.
(13) Fadeeva, E.; Truong, V. K.; Stiesch, M.; Chichkov, B. N.; Crawford, R. J.; Wang, J.; Ivanova, E. P. Bacterial Retention on Superhydrophobic Titanium Surfaces Fabricated by Femtosecond Laser Ablation. *Langmuir* **2011**, *27*, 3012−3019.
(14) Whitehead, K. A.; Colligon, J.; Verran, J. Retention of Microbial Cells in Substratum Surface Features of Micrometer and Sub-Micrometer Dimensions. *Colloids Surf., B* **2005**, *41*, 129−138.
(15) Kargar, M.; Wang, J.; Nain, A. S.; Behkam, B. Controlling Bacterial Adhesion to Surfaces Using Topographical Cues: A Study of the Interaction of *Pseudomonas aeruginosa* with Nanofiber-Textured Surfaces. *Soft Matter* **2012**, *8*, 10254−10259.
(16) Ye, Z.; Ellis, M. W.; Nain, A. S.; Behkam, B. Effect of Electrode Sub-Micron Surface Feature Size on Current Generation of *Shewanella oneidensis* in Microbial Fuel Cells. *J. Power Sources* **2017**, *347*, 270−276.
(17) Epstein, A. K.; Hochbaum, A. I.; Kim, P.; Aizenberg, J. Control of Bacterial Biofilm Growth on Surfaces by Nanostructural Mechanics and Geometry. *Nanotechnology* **2011**, *22*, No. 494007.
(18) Whitehead, K. A.; Verran, J. The Effect of Surface Topography on the Retention of Microorganisms. *Food Bioprod. Process.* **2006**, *84*, 253−259.
(19) Magin, C. M.; Cooper, S. P.; Brennan, A. B. Non-Toxic Antifouling Strategies. *Mater. Today* **2010**, *13*, 36−44.
(20) Renner, L. D.; Weibel, D. B. Physicochemical Regulation of Biofilm Formation. *MRS Bull.* **2011**, *36*, 347−355.
(21) Teughels, W.; Assche, N.; Sliepen, I.; Quirynen, M. Effect of Material Characteristics And/or Surface Topography on Biofilm Development. *Clin. Oral Implant. Res.* **2006**, *17*, 68−81.
(22) Dobosz, K. M.; Kolewe, K. W.; Schiffman, J. D. Green Materials Science and Engineering Reduces Biofouling: Approaches for Medical and Membrane-Based Technologies. *Front. Microbiol.* **2015**, *6*, No. 196.
(23) Pogodin, S.; Hasan, J.; Baulin, V. A.; Webb, H. K.; Truong, V. K.; Phong Nguyen, T. H.; Boshkovikj, V.; Fluke, C. J.; Watson, G. S.; Watson, J. A.; Crawford, R. J.; Ivanova, E. P. Biophysical Model of Bacterial Cell Interactions with Nanopatterned Cicada Wing Surfaces. *Biophys. J.* **2013**, *104*, 835−840.
(24) Nowlin, K.; Boseman, A.; Covell, A.; Lajeunesse, D. Adhesion-Dependent Rupturing of *Saccharomyces cerevisiae* on Biological Antimicrobial Nanostructured Surfaces. *J. R. Soc., Interface* **2015**, *12*, No. 20140999.
(25) Hermansson, M. The DLVO Theory in Microbial Adhesion. *Colloids Surf., B* **1999**, 105−119.
(26) Zita, A.; Hermansson, M. Effects of Ionic Strength on Bacterial Adhesion and Stability of Flocs in a Wastewater Activated Sludge System. *Appl. Environ. Microbiol.* **1994**, *60*, 3041−3048.
(27) Rijnaarts, H. H. M.; Norde, W.; Lyklema, J.; Zehnder, A. J. B. DLVO and Steric Contributions to Bacterial Deposition in Media of Different Ionic Strengths. *Colloids Surf., B* **1999**, *14*, 179−195.
(28) Bolster, C. H.; Mills, A. L.; Hornberger, G. M.; Herman, J. S. Effect of Surface Coatings, Grain Size, and Ionic Strength on the Maximum Attainable Coverage of Bacteria on Sand Surfaces. *J. Contam. Hydrol.* **2001**, *50*, 287−305.
(29) Truesdail, S. E.; Lukasik, J.; Farrah, S. R.; Shah, D. O.; Dickinson, R. B. Analysis of Bacterial Deposition on Metal (Hydr)oxide-Coated Sand Filter Media. *J. Colloid Interface Sci.* **1998**, *203*, 369−378.
(30) Chang, Y.-I.; Chang, P.-K. The Role of Hydration Force on the Stability of the Suspension of *Saccharomyces cerevisiae*-application of the Extended DLVO Theory. *Colloids Surf., A* **2002**, *211*, 67−77.
(31) Claesson, P.; Carmona-Ribeiro, A. M.; Kurihara, K. Dihexadecyl Phosphate Monolayers: Intralayer and Interlayer Interactions. *J. Phys. Chem.* **1989**, *93*, 917−922.
(32) Bayoudh, S.; Othmane, A.; Mora, L.; Ben Ouada, H. Assessing Bacterial Adhesion Using DLVO and XDLVO Theories and the Jet Impingement Technique. *Colloids Surf., B* **2009**, *73*, 1−9.
(33) Vilinska, A.; Hanumantha Rao, K. Surface Thermodynamics and Extended DLVO Theory of *Acidithiobacillus ferrooxidans* Cells Adhesion on Pyrite and Chalcopyrite. *Open Colloid Sci. J.* **2009**, *2*, 1−14.
(34) van Oss, C. J. Hydrophobicity of Biosurfaces - Origin, Quantitative Determination and Interaction Energies. *Colloids Surf., B* **1995**, *5*, 91−110.
(35) Bos, R.; van der Mei, H. C.; Busscher, H. J. Physico-Chemistry of Initial Microbial Adhesive Interactions - Its Mechanisms and Methods for Study. *FEMS Microbiol. Rev.* **1999**, *23*, 179−230.
(36) Absolom, D. R.; Lamberti, F. V.; Policova, Z.; Zingg, W.; van Oss, C. J.; Neumann, A. W. Surface Thermodynamics of Bacterial Adhesion. *Appl. Environ. Microbiol.* **1983**, *46*, 90−97.
(37) Busscher, H. J.; Weerkamp, A. H.; van der Mei, H. C.; van Pelt, A. W.; de Jong, H. P.; Arends, J. Measurement of the Surface Free Energy of Bacterial Cell Surfaces and Its Relevance for Adhesion. *Appl. Environ. Microbiol.* **1984**, *48*, 980−983.
(38) Busscher, H. J.; Norde, W.; Sharma, P. K.; van der Mei, H. C. Interfacial Rearrangement in Initial Microbial Adhesion to Surfaces. *Curr. Opin. Colloid Interface Sci.* **2010**, *15*, 510−517.
(39) Decuzzi, P.; Ferrari, M. Modulating Cellular Adhesion through Nanotopography. *Biomaterials* **2010**, *31*, 173−179.
(40) Gulati, M.; Nobile, C. J. *Candida albicans* Biofilms: Development, Regulation, and Molecular Mechanisms. *Microbes Infect.* **2016**, *18*, 310−321.
(41) Kojic, E. M.; Darouiche, R. O. *Candida* Infections of Medical Devices. *Clin. Microbiol. Rev.* **2004**, *17*, 255−267.
(42) Chandra, J.; Kuhn, D. M.; Mukherjee, P. K.; Hoyer, L. L.; McCormick, T.; Ghannoum, M. A. Biofilm Formation by the Fungal Pathogen *Candida albicans*: Development, Architecture, and Drug Resistance. *J. Bacteriol.* **2001**, *183*, 5385−5394.
(43) Seifert, U.; Lipowsky, R. Adhesion of Vesicles. *Phys. Rev. A* **1990**, *42*, 4768−4771.
(44) Deserno, M.; Gelbart, W. Adhesion and Wrapping in Colloid-Vesicle Complexes. *J. Phys. Chem. B* **2002**, 5543−5552.
(45) Helfrich, W. Elastic Properties of Lipid Bilayers: Theory and Possible Experiments. *Z. Naturforsch., C: J. Biosci.* **1973**, *28*, 693−703.
(46) Salez, T.; Benzaquen, M.; Raphaël, É. From Adhesion to Wetting of a Soft Particle. *Soft Matter* **2013**, *9*, No. 10699.
(47) Sundstrom, P. Adhesins in *Candida albicans*. *Curr. Opin. Microbiol.* **1999**, 353−357.
(48) Comyn, J. *Adhesion Science*, RSC Paperbacks; The Royal Society of Chemistry: Cambridge, U.K., 1997.
(49) Owens, D. K.; Wendt, R. C. Estimation of the Surface Free Energy of Polymers. *J. Appl. Polym. Sci.* **1969**, *13*, 1741−1747.
(50) Dietrich, C.; Angelova, M.; Pouligny, B. Adhesion of Latex Spheres to Giant Phospholipid Vesicles: Statics and Dynamics. *J. Phys. II* **1997**, *7*, 1651−1682.
(51) Smith, A. E.; Zhang, Z.; Thomas, C. R.; Moxham, K. E.; Middelberg, A. P. The Mechanical Properties of *Saccharomyces cerevisiae*. *Proc. Natl. Acad. Sci. U.S.A.* **2000**, *97*, 9871−9874.
(52) Fradin, C.; Satsoura, D.; Andrews, D. W. *Biomembrane Frontiers: Nanostructures, Models, and the Design of Life*, 1st ed.; Jue, T.; Risbud, S. H.; Longo, M. L.; Faller, R., Eds.; Humana Press, 2009.
(53) Simonin, H.; Beney, L.; Gervais, P. Sequence of Occurring Damages in Yeast Plasma Membrane during Dehydration and Rehydration: Mechanisms of Cell Death. *Biochim. Biophys. Acta, Biomembr.* **2007**, *1768*, 1600−1610.
(54) Nain, A. S.; Sitti, M.; Jacobson, A.; Kowalewski, T.; Amon, C. Dry Spinning Based Spinneret Based Tunable Engineered Parameters (STEP) Technique for Controlled and Aligned Deposition of Polymeric Nanofibers. *Macromol. Rapid Commun.* **2009**, *30*, 1406−1412.
(55) Nain, A. S.; Wang, J. Polymeric Nanofibers: Isodiametric Design Space and Methodology for Depositing Aligned Nanofiber Arrays in Single and Multiple Layers. *Polym. J.* **2013**, *45*, 695.

DOI: 10.1021/acsami.8b02907
ACS Appl. Mater. Interfaces 2018, 10, 15477−15486

(56) Wang, J.; Nain, A. S. Suspended Micro/Nanofiber Hierarchical Biological Scaffolds Fabricated Using Non-Electrospinning STEP Technique. *Langmuir* **2014**, *30*, 13641−13649.
(57) Flores-Mireles, A. L.; Walker, J. N.; Caparon, M.; Hultgren, S. J. Urinary Tract Infections: Epidemiology, Mechanisms of Infection and Treatment Options. *Nat. Rev. Microbiol.* **2015**, *13*, 269−284.
(58) Gillum, A. M.; Tsay, E. Y.; Kirsch, D. R. Isolation of the *Candida albicans* Gene for Orotidine-5′-phosphate Decarboxylase by Complementation of *S. cerevisiae* ura3 and *E. coli* pyrF Mutations. *Mol. Genet. Genomics* **1984**, *198*, 179−182.
(59) Chandra, J.; Mukherjee, P. K.; Ghannoum, M. A. In Vitro Growth and Analysis of *Candida* Biofilms. *Nat. Protoc.* **2008**, *3*, 1909−1924.
(60) Honraet, K.; Goetghebeur, E.; Nelis, H. J. Comparison of Three Assays for the Quantification of *Candida* Biomass in Suspension and CDC Reactor Grown Biofilms. *J. Microbiol. Methods* **2005**, *63*, 287−295.
(61) Sharma, P. K.; Hanumantha Rao, K. Analysis of Different Approaches for Evaluation of Surface Energy of Microbial Cells by Contact Angle Goniometry. *Adv. Colloid Interface Sci.* **2002**, *98*, 341−463.
(62) Dague, E.; Bitar, R.; Ranchon, H.; Durand, F.; Yken, H. M.; François, J. M. An Atomic Force Microscopy Analysis of Yeast Mutants Defective in Cell Wall Architecture. *Yeast* **2010**, *27*, 673−684.
(63) Ene, I. V.; Adya, A. K.; Wehmeier, S.; Brand, A. C.; Maccallum, D. M.; Gow, N. A. R.; Brown, A. J. Host Carbon Sources Modulate Cell Wall Architecture, Drug Resistance and Virulence in a Fungal Pathogen. *Cell. Microbiol.* **2012**, *14*, 1319−1335.
(64) Liu, Y.; Zhao, Q. Influence of Surface Energy of Modified Surfaces on Bacterial Adhesion. *Biophys. Chem.* **2005**, *117*, 39−45.

DOI: 10.1021/acsami.8b02907
ACS Appl. Mater. Interfaces 2018, 10, 15477−15486